Turbulence Simulations of Transonic Flows over an NACA-0012 Airfoil

P. Balakumar
Flow Physics and Control Branch, NASA LaRC, MS 170, Hampton, VA 23681-2199
Email: ponnampalam.balakumar-1@nasa.gov, (757) 864-8453

Prahladh Iyer
National Institute of Aerospace, Hampton, VA
Email: prahladh.s.iyer@nasa.gov, (757) 864-4045

Mujeeb R. Malik
Computational Aerosciences Branch, NASA LaRC, Hampton, VA 23681-2199
Email: m.r.malik@nasa.gov, (757) 864-6228

Three different simulation approaches, namely unsteady Reynolds-averaged Navier-Stokes (URANS), delayed detached-eddy simulation (DDES), and wall-modeled large-eddy simulation (WMLES) are employed to simulate transonic flow over an NACA-0012 airfoil at different angles of attack covering pre- and post-buffet-onset regimes. The freestream Mach number is 0.75, and the Reynolds number based on the chord length is 10 million. These conditions are the same as the wind-tunnel experimental conditions of McDevitt and Okuno (1985).[1] The NASA FUN3D solver is used for the simulations, which is an unstructured, compressible flow solver. The URANS simulations are performed using the Spalart-Allmaras (SA) model with the compressibility correction, the DDES predictions are based on the SA model, and the WMLES are performed using an equilibrium wall-model. The unsteady RANS simulations, only with the compressibility correction, predict the pre- and post- buffet characteristics, which compare well with the experimental results. DDES results predicted a lower buffet onset angle compared to experiment. The predicted shock locations are upstream of the locations predicted by URANS. Using a fine grid in the spanwise direction, WMLES predictions show buffeting consistent with the experiment.

I. Introduction

Transonic flows over wing surfaces are characterized by the formation of a supersonic region on the forward portion, followed by a shock, which increases the wave drag and causes the flow to separate. At small angles of attack, the shock is quasisteady. Beyond a critical angle, the shock moves periodically upstream and downstream at a fixed frequency. Because of this phenomenon, the lift and drag over the wing also oscillate periodically. This causes structural vibrations, "buffeting", and affects the performance of the aircraft. At high Reynolds numbers, the flow is fully turbulent starting from the leading edge, where the boundary layer is very thin. When the turbulent boundary layer interacts with the shock, the boundary layer thickness increases, high intensity oscillations develop, and shock-induced separation occurs. With increasing angle of attack, the flow becomes unsteady in the mean and buffeting commences. Understanding the mechanisms and predicting the critical buffeting conditions numerically are difficult due to the sensitivity of this phenomena to turbulent models, numerical algorithms, grid topology, and other factors.

Experimental, theoretical, and numerical investigations of transonic shock buffeting have been performed for several decades. A comprehensive review is given in an excellent article by Giannelis et al. (2017).[2] The review article by Lee (2001)[3] summarizes the early work on identifying the mechanisms for buffeting. Most of the transonic-buffet experiments were conducted using low-aspect ratio two-dimensional wings, such as the RA16SC1[4], NACA-0012[1], NACA-64A204[5], and OAT15[6]. Several numerical simulations using unsteady Reynolds-averaged Navier-Stokes (URANS)[7-9], delayed detached eddy simulation (DDES)[10-12], and recently wall-resolved[13] and wall-modeled[14] large-eddy simulation (WRLES, WMLES) have been performed.

McDevitt and Okuno (1985)[1] conducted an experiment to study the transonic buffet problem over a NACA0012 airfoil at high Reynolds numbers and at high subsonic Mach numbers. Pressure distributions were measured at selected angles of attack and pressure sensors were used to detect the onset of large unsteady oscillations on the surface of the

airfoil. A very detailed experiment was recently performed over an OAT15A airfoil at a transonic Mach number of 0.73 and chord Reynolds number of 3 million.[6] Pressure distributions, mean velocity profiles, and turbulent intensities were also measured.

Two possible mechanisms are proposed to explain the sustained shock oscillations over supercritical airfoils at transonic speeds. One mechanism[15] is that when eddies generated downstream of the shock foot convect over the trailing edge of the airfoil, acoustic waves are emanated from the trailing edge. These waves propagate upstream and interact with the shock and generate disturbances at the foot of the shock. Another mechanism is that the whole system is globally unstable to small perturbations. Crouch et al. (2009)[16] successfully predicted the experimentally measured onset boundary curve for the flows over NACA0012[1] and the OAT15A[6] airfoils using this method.

Goncalves et al. (2004)[8] assessed the accuracy of different turbulence models in predicting the shock induced oscillations (SIO) for flow over an RA16SC1 airfoil using URANS. Several two-equations turbulence models and the one equation SA model were tested in the simulations. The frequency of shock oscillations and the amplitude variations of the lift coefficients were computed at three angles of attack corresponding to the buffet onset, buffet exit, and in between. The computed results were compared with the experimental results. The conclusion was that the basic models do not predict the shock-buffeting consistently. Modified versions of the models were able to capture the onset, offset, and the stable shock-buffeting favorably. However, the predicted shock oscillating frequency and the lift amplitudes differ from the experimental values. One of the important observations from Crouch (2009)[16] global linear stability calculations is that the compressibility correction to the SA equation was needed to obtain unstable solutions for the flows over NACA0012 airfoils. Similar observations were made in other URANS simulations.[7, 9, 12]

Iovnovich et al. (2012)[9] performed URANS simulations for the experimental cases of McDevitt and Okuno (1985)[1] using SA turbulence model with Edward and Chandra's[17] modifications. They presented the shock-buffet onset boundary and compared favorably with the experimental[1] results. They also showed the simulation results at a Mach number of 0.72 and at three angles of attacks 4.6, 6.0, and 9.0 degrees. These angles correspond to the buffet onset, to a well developed buffet case, and to the buffet offset conditions, respectively. Based on the results, it was concluded that the buffet onset angles and the buffet frequencies could be predicted using URANS with a suitable RANS model. The buffet offset angles and the amplitudes of oscillations were not well predicted by the URANS. The flow fields for the well developed buffet case showed that the buffet is initiated by the shock/separation bubble interactions.

The objective of this work is to investigate the prediction of transonic buffet using URANS and eddy resolving methods (both DDES and WMLES) for flows over an NACA-0012 airfoil. Simulations were performed using the unstructured finite volume FUN3D code (https://fun3d.larc.nasa.gov) at a Reynolds number of $Re_c = 10*10^6$ and at a Mach number of 0.75. These conditions are the same as the experimental conditions of McDevitt and Okuno (1985).[1] URANS simulations were performed first at different angles of attack to explore the feasibility of this approach in predicting shock-buffeting. Secondly, eddy resolving DDES and WMLES predictions were performed at pre- and post-buffeting angles of attack to investigate the capability of eddy-resolving methods to predict shock-buffeting.

II. Solution algorithm

Computations are performed using the FUN3D code (https://fun3d.larc.nasa.gov), which is a node-centered finite-volume code developed at the NASA Langley Research Center that solves the three-dimensional compressible Navier-Stokes equations on unstructured computational grids.[18, 19] The grids may contain tetrahedra, pyramids, prisms, and hexahedra. Volume integrals are performed over the median-dual around a node. Roe's flux difference splitting is used for the calculation of the inviscid term. The numerical fluxes across the dual faces are obtained using the Roe's approximate Riemann solver.[20] The primitive variables on the left and the right sides of a cell face are obtained using an unstructured monotonic upstream scheme for conservation laws (UMUSCL).[21, 22] The UMUSCL free parameter, kappa, is selected to be 0.5 in the URANS simulations and is set to 0.9 for the DDES and WMLES predictions to reduce numerical dissipation. For discretization of the viscous fluxes, the Green-Gauss theorem is used to compute cell-based gradients. The viscous fluxes are second-order accurate on general mixed-element grids and the solution is advanced in time using 2nd-order backward-Euler implicit scheme. The Van Albada limiter is used in the simulations. The code has been validated previously for complex flows with a broad range of capabilities ranging from steady-state Reynolds-averaged Navier-Stokes (RANS), adjoint-based optimization, fluid-structure interaction, grid adaptation, and Detached-Eddy Simulation (DES). Recently, WMLES capabilities have been added in FUN3D and assessed for canonical 2D geometries and for 3D geometries.[23]

III. Results

A. URANS

The URANS simulations are performed using the Spalart-Allmaras (SA) model.[24] Computations were performed using different modifications, curvature correction) (RC),[25] nonlinear quadratic constitutive relations (QCR),[26] and the compressibility corrections.[27] The model equations and the model parameters are given in the turbulence modeling resource (TMR) webpage (https://turbmodels.larc.nasa.gov). It was found that the compressibility correction is needed to capture buffet phenomena above a critical angle of attack. Hence all unsteady results are presented for the SA model with the compressibility correction. The compressibility correction is a destructive term added on the right-hand side of the SA model to reduce the eddy viscosity in a mixing layer.

1. *Grids*

Both structured and an unstructured grids are employed in the simulations. The topologies of the coarser structured and the finer unstructured grids are shown in Figs. 1(a) and (b), respectively. The unstructured grid consists of hexes and prisms. The grid is clustered near the wall and is made isotropic in the outer part as shown in Fig. 1(b). The wall spacing near the wall for both grids is about 1×10^{-6} which gives a $y^+ < 0.5$ across the wing. The grid is refined in the middle part of the wing to capture the shock oscillations accurately. The grid size in the middle part of the wing is about $\Delta x = 0.002c$, where c is the chord length. The outer boundary is located at $100c$ from the center of the wing. The coarser and the finer grids consist of 23K and 0.23M nodes, respectively.

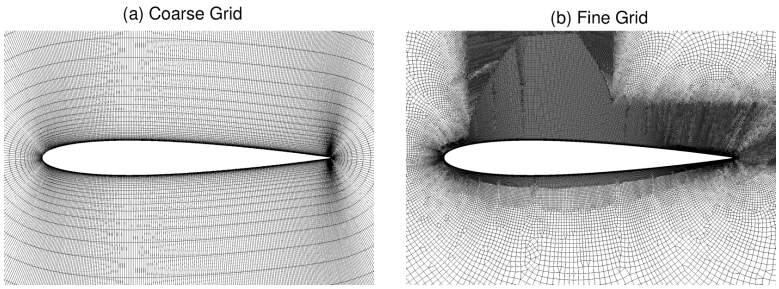

Fig. 1 Coarse and fine grid topologies.

2. *URANS Results*

URANS were performed using the SA model with compressibility correction for flow over an NACA-0012 airfoil at a chord Reynolds number of $Re_c = 10 \times 10^6$ and free stream Mach number of 0.75. Simulations were performed at increasing angles of attack from $\alpha = 0$ to 6 degrees. Figure 2 shows the variation of the lift coefficient (C_L) with the nondimensional time $t = t^*U_\infty/c$ for increasing angles of attack from 3.5 to 5.5 deg. The lift reaches a steady value below a critical angle of attack and attains a periodic cycle above it. The critical angle was found to be about 3.8 degrees, which is close to the experimental buffet onset angle of 3.4 degrees at this Mach number. The maximum lift oscillations occur around 4.5 degrees angle of attack and then the lift returns to a steady value near 5 degrees angle of attack. This shows that the flow field is unstable in a narrow range of angles of attack. As the angle of attack increases, the flow separation point moves closer to the leading edge and at 5.5 degrees, is located closer to $x/c = 0.2$. Iovnovich et al. (2012)[9] also observed that at the buffet offset conditions the shock moves closer to the leading edge and the flow is separated from the foot of the shock to the trailing edge. Average lift coefficients, change in the lift coefficients, and the periods of oscillations are given in Table 1. At 4.0 and 4.5 degrees angles of attack, the average lift coefficient is approximately 0.50, and the amplitudes of the lift oscillations, ΔC_L, are 0.08 and 0.10, respectively. The period of oscillations, T, are about 16.6 and 15.7 at these angles, respectively, and the corresponding Strohaul numbers are $St = 0.38$ and 0.40, which are smaller than the experimental value of 0.47 measured at 4.0 degrees angle of attack. These numbers compare well with the values of $St = 0.38$ and $\Delta C_L = 0.05$ predicted by Iovnovich et al. (2012)[9] at an angle of attack of 4 degrees. Figure 3(b) shows the variation of the lift coefficient obtained with the fine and the coarse grids. Compared to the fine grid, the oscillations predicted using the coarse grid are lower. Figure 4 shows variations in the lift coefficient for simulations performed with increasing nondimensional timesteps $dt = 0.0005$, 0.001, and 0.005. These timesteps correspond to approximately 2660, 1330, and 270 steps per one convective time c/U_∞. The results agree for the three timesteps, but with the higher timesteps larger subiterations are needed to

obtain 5 orders of magnitude reduction in the residuals. These results show that URANS using the SA model with the compressibility correction captures the transonic buffet over the NACA0012 airfoils accurately.

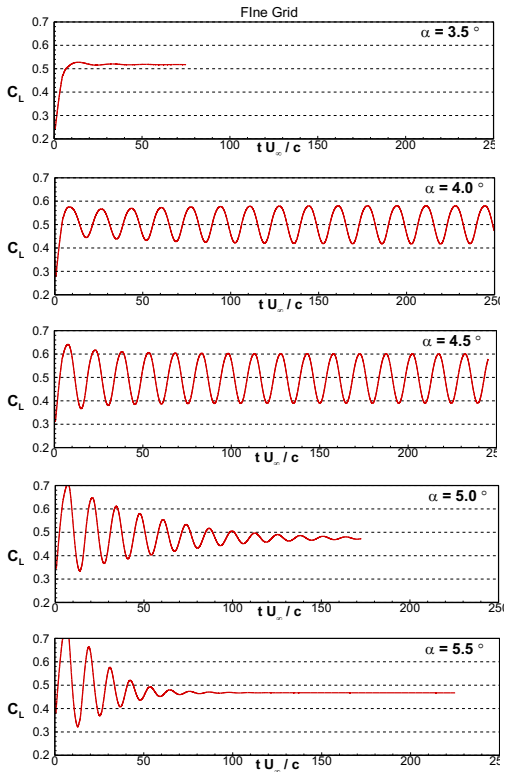

Fig. 2 Variation of lift coefficient with time for $\alpha = 3.5°$ to $5.5°$.

Table 1. Statistical properties of the lift variation

α (deg)	C_L	ΔC_L	T	St
3.5	0.50	0.00		
4.0	0.50	0.08	16.6	0.38(0.47 Exp.)
4.5	0.50	0.10	15.7	0.40
5.0	0.48	0.005	15.0	0.40
5.5	0.48	0.00		

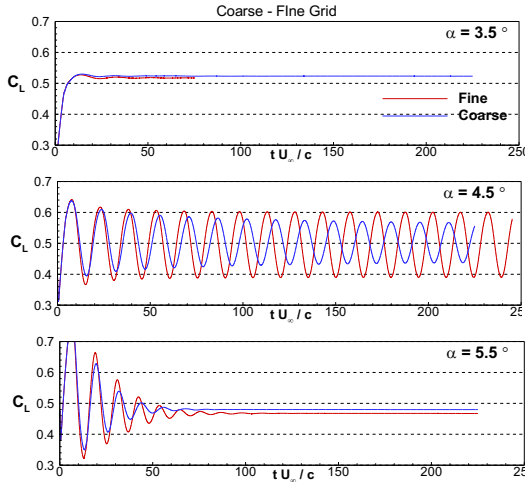

Fig. 3 Variations of lift coefficient with the flow through time obtained with the coarse and fine grids.

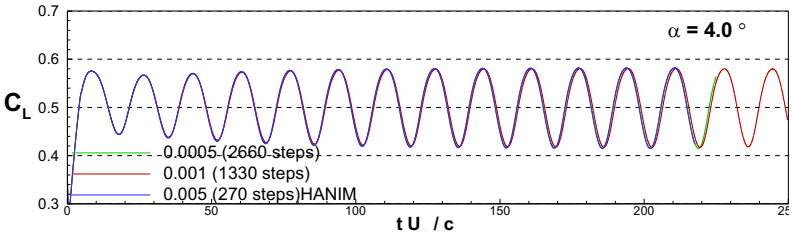

Fig. 4 Variations of lift coefficient with the flow through time at different timesteps obtained using URANS at 4°.

Figure 5 shows instantaneous streamwise velocity (*u*-velocity) contours during one cycle of the shock motion at 4.5 degrees. The starting time of the cycle (t = 0T) is defined as the time when the shock is at the furthest downstream position. The sequence is shown at four phases t = 0, 1/4, 1/2, and 3/4 T in the cycle. At the starting phase t = 0T, the shock is at x/c = 0.38, where x is the streamwise distance from the leading edge of the wing. There exists a small separation bubble at the foot of the shock. With increasing time, the shock moves upstream and a large separation bubble forms at the foot of the shock and extends to the trailing edge of the wing, Fig.5(b). At the half period of the cycle, Fig. 5(c), the shock reaches the furthest upstream location, x/c = 0.24, and the height of the separation bubble becomes smaller at the foot and larger near the trailing edge. In the next phase, Fig. 5(d), the shock starts to move downstream and the height of the separation bubble becomes smaller both at the foot and at the trailing edge. This cycle continues periodically with a long period of T = 15.7 c/U_∞. These observations were also made by Iovnovich et al. (2012)[9] and Raghunathan et al.[28] It appears that the separation bubbles that form at the foot of the shock and at the trailing edge merge and split during one buffet cycle.

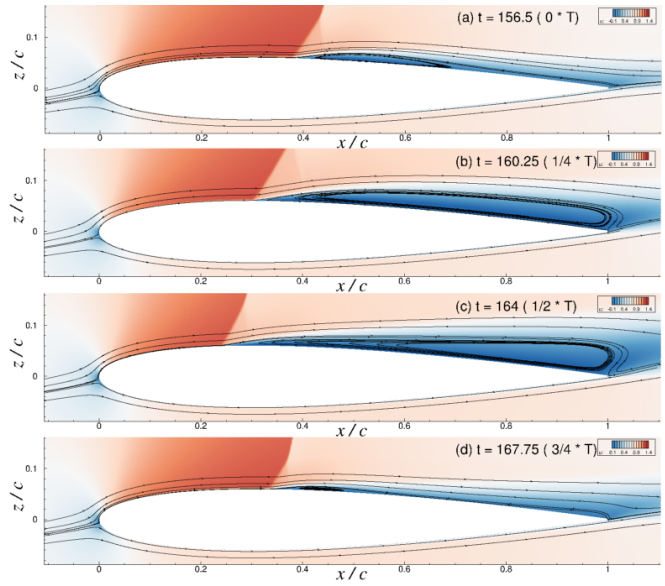

Fig. 5 Streamwise velocity contours during one cycle of the shock motion for $\alpha = 4.5°$ (t = 0, 1/4, 1/2, 3/4 T).

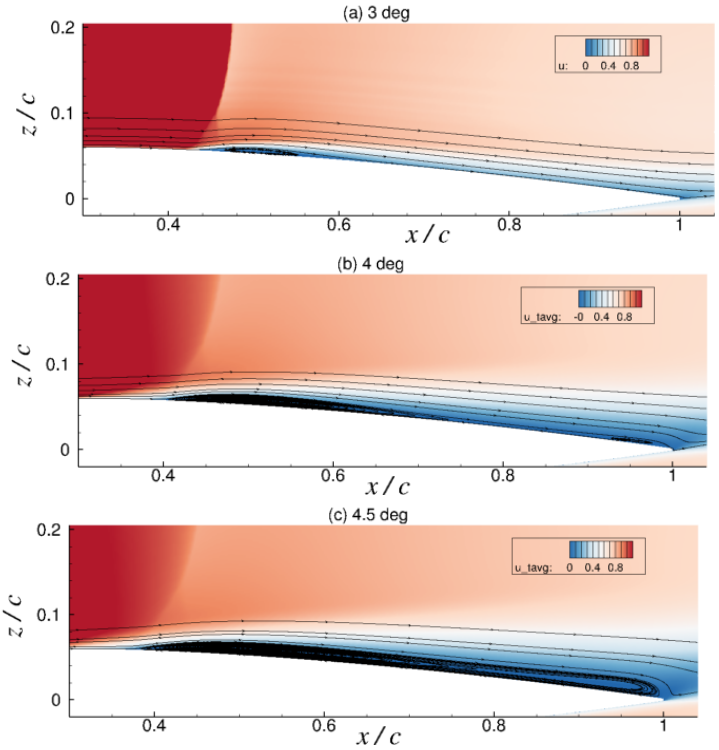

Fig. 6 Time averaged velocity contours for $\alpha = 3.0°, 4.0°, and\ 4.5°$.

Figures 6(a-c) display the time-averaged *u*-velocity contours and streamlines at angles of attack of 3, 4 and 4.5 degrees. URANS predicts a steady flow field at 3 degrees. The flow field consists of a small separation bubble at the foot of the shock and an attached boundary layer all the way to the trailing edge. The flow field for the angle of attack of 4 degrees shows a larger separation bubble at the foot of the shock and a small bubble near the trailing edge. Figure 6(c) shows the velocity contours for the angle of attack of 4.5 dgrees. The bubbles at the foot and at the trailing edge merge and form a large separation bubble that extends from the root to the trailing edge. Figures 7(a) and (b) show pressure distributions at angles of attack 2, 3, 3.5, 4 and 4.5 degrees. In Fig. 7(a), the pressure distributions for the angle of attack of 2 degrees are compared with the experimental results of McDevitt and Okuno (1985).[1] The

agreement between the URANS and the experiment is very good. It is seen in Fig. 7(b) that the shock reaches the furthest point along the wing to $x/c \sim 0.42$ at 3 degrees and moves slowly upstream with increasing angles of attack. This observation agrees with the experiment of McDevitt and Okuno (1985).[1] It was also observed in the experiment that the shock oscillations start to occur near an angle of attack of 3 degrees. It is also observed in Fig. 7(b) that the pressure distributions for the angles of attack of 4 and 4.5 degrees are smeared due to the oscillations of the shock.

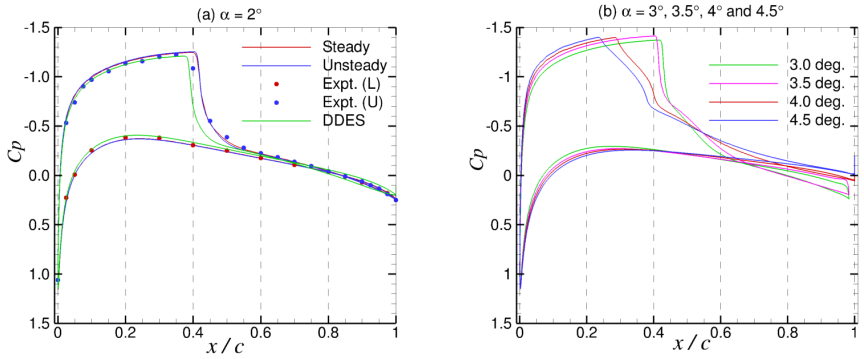

Fig. 7 Pressure coefficients distributions at different angles of attack, (a) $\alpha = 2.0°$ and (b) $\alpha = 3.0°, 3.5°, 4.0°,$ and $4.5°$.

Figures 8(a) and (b) display the contours of the root mean square (rms) of the pressure and *u*-velocity fluctuations, respectively, for an angle of attack of 4.5 degrees. As expected, larger pressure fluctuations are observed across the shock oscillations region. Pressure fluctuations are also observed downstream of the shock above the wing. It is also seen that the pressure fluctuations extend around the trailing edge and over the lower surface of the airfoil. The structure of the rms pressure agrees well with the eigenfunctions distributions computed using the global stability analysis.[16] Due to the movement of the separation bubble during the buffeting, large velocity fluctuations are observed from the root of the shock to the trailing edge.

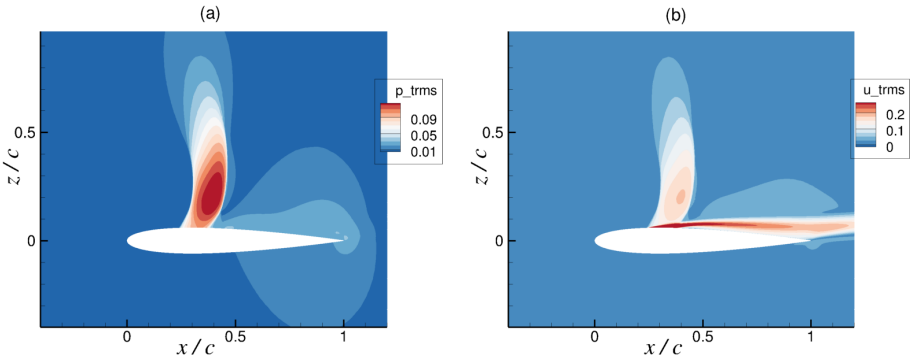

Fig. 8 Root mean square of (a) pressure and (b) u-velocity fluctuations at $\alpha = 4.5°$.

Figures 9 and 10 show the boundary layer mean *u*-velocity profiles and turbulent quantities at stations upstream and downstream of the shock for angles of attack of 3 and 4.5 degrees. The velocity and turbulence quantities are normalized by the freestream velocity, U_∞. Figures 9(a) and 10(a) show the mean velocity profiles, Figs. 9(b) and 10(b) depict the turbulent intensities, and Figs. 9(c) and 10(c) display the eddy-viscosity coefficients. Figure 10(b) shows the resolved and instantaneous modeled normal turbulent stress $\langle u'u' \rangle$. Figure 10(c) displays the eddy-viscosity distributions at different stations when the shock is furthest upstream (solid) and downstream (dash). Similarly, Fig. 11 shows the instantaneous velocity profiles when the shock is at the furthest upstream and downstream positions. The first observation is that the boundary layer is very thin upstream of the shock and is several times thicker downstream. The boundary layer thickness is 0.004 at $x/c = 0.20$ and approximately 0.03 at $x/c = 0.6$ for an angle of attack of 3 degrees. The boundary layer thickness is 0.006 and 0.07 at these locations for an angle of attack of 4.5 degrees, respectively. The eddy viscosity is on the order of 50-100 upstream of the shock and is about 1000-3000 downstream of the shock at an angle of attack of 3 degrees. The eddy viscosity is about 100 upstream and is about

10000 downstream of the shock when the shock is at the furthest upstream location for an angle of attack of 4.5 degrees. The turbulent stress distributions show the typical profiles for a turbulent boundary layer at 3 degrees. The normal stress distributions at 4.5 degrees show almost the same amplitudes for the resolved part and the modeled part when the shock is at the furthest upstream location except near the shock location $x/c = 0.4$. Figures 11 shows that the velocity profiles are very inflectional due to the separation region when the shock is located at the furthest upstream. The boundary layer thickness increases by about two times during the buffeting cycle. The eddy viscosity also changes by about two times during the oscillation of the shock. These observations will become important when eddy resolving methods are used to predict the buffeting at transonic speeds.

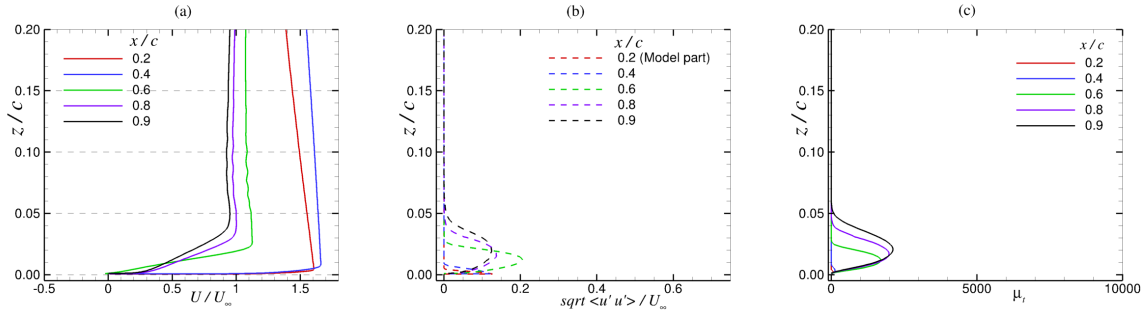

Fig. 9 Profiles of (a) mean u-velocity, (b) normal turbulent stresses, and (c) eddy-viscosity at $\alpha = 3.0°$.

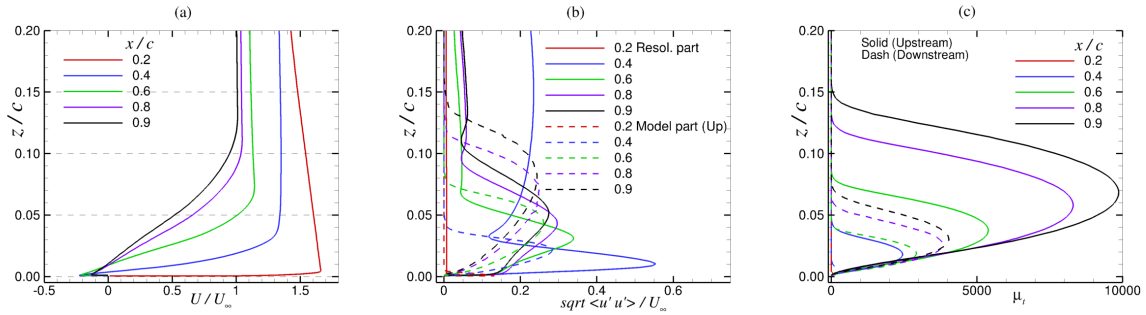

Fig. 10 Profiles of (a) mean u-velocity, (b) normal turbulent stresses, and (c) eddy-viscosity at $\alpha = 4.5°$.

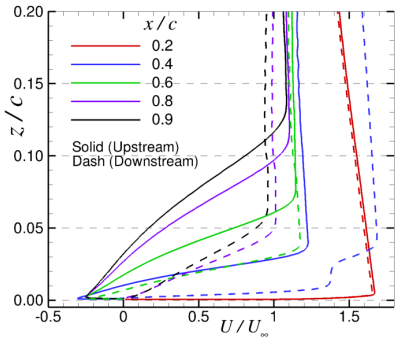

Fig. 11 Profiles of u-velocity when the shock is at the furthest upstream and downstream at $\alpha = 4.5°$.

B. DDES

Detached eddy simulations were performed using the FUN3D for pre- and post-buffet onset angles of attack of 2, 3 and 4 degrees. Computations were performed using SA–based, delayed-detached-eddy-simulation.[29] Details about

the model and the implementation of DDES in FUN3D are given in Vatsa et al. (2017).[30] In the RANS and URANS methods, effects of turbulence are fully captured by the turbulence model used. The RANS computations predict the flow field satisfactorily in attached boundary layers, but they can perform poorly where the flow is separated. The detached-eddy-simulations (DES) method[31] was designed to improve the prediction of separated flows. The length scale in the base turbulence model is reduced based on the grid size to change the model to run in the Large-eddy-simulation (LES) mode in the massively separated region. Hence in this method, the flow field in the attached region is resolved using RANS, and the separated region is simulated by the LES. At the interface region from RANS to LES, turbulence is expected to be generated by the strong instability of the shear layer that forms near the separation point. However, it has been observed that DES can predict spurious separated flow regions in attached regions when the grid is refined. The model switches to the LES mode due to the fine grid, but fluctuations generated at the interface are not sufficient to balance the turbulent stresses modeled by the RANS. The depleted Reynolds stresses induce unwanted separation. DDES[31] was developed to overcome this issue by shielding the attached boundary layer to remain in the RANS mode. In mildly separated flows, for example flows over a wing at high angles of attack or flows over wings with shocks, the flow separates on the aft part of the wing or at the foot of the shock and forms thin separation bubbles inside the boundary layer. The question is how does the DDES method perform in these situations?

DDES has been used for prediction of buffet onset for flow over the OAT15 airfoil, Grossi et al. (2017). Deck et al. (2015) used zonal-DES where the shock-boundary layer region is forced to be in the RANS mode to predict the transonic buffet for the flow over the OAT15A airfoil. The DDES predictions agree better with the experimental results than the DES, however, the predicted shock locations were further upstream than those in the experiment. The predicted pressure distributions also show a plateau in the downstream region compared to the experiment. An improved version of the DDES, IDDES, was employed to predict the transonic buffeting for flows over NACA0012[12] and OAT15A[32] airfoils. The predicted lift coefficient for the NACA0012 at the post buffet onset angle of 4 degrees is much lower than the URANS predicted value. The same behavior is observed in the prediction of shock location in the flow over the OAT15A airfoil. The shock is further upstream of the experimental value and the flow field shows a large separation bubble downstream of the shock.[32]

In the present DDES predictions, the grid in the x-z plane is the same as the fine grid used in the URANS simulations, Fig. 1(b). However, the grid is protruded in the spanwise direction uniformly to a domain size of 0.1c, with 51 points. The grid is isotropic in the x and z directions in the middle part of the wing with an approximate grid size of $0.002c$. The overall grid consists of 11.8M nodes. In the DDES implementation, the Des-length scale Δ is taken as the maximum edge-length at a particular node. The Des-constant C_{DES} is chosen to be 0.65. The turbulent variable in the SA model in the freestream is set to three times the kinematic viscosity in the simulation. The low-dissipation parameter kappa is set to 0.9 and the 'hvanalbata' limiter is used in the simulations to reduce the oscillations near the shock. A nondimensional time step of $dt\ U_\infty/c$ = 0.00075 is used in the unsteady simulations. A five order-of-magntitude reduction in the subiterations is observed in the residuals with 10 subiterations cycles.

Figure 12 shows the variation of the lift coefficient with the nondimensional time obtained from the DDES predictions for an angle of attack of 4 degrees. The results from the URANS computations are also included for comparison. The lift oscillations from the DDES predictions show buffeting as observed in the URANS, but they are not as periodic as the URANS. Very low frequency oscillations with a period of about 60 are also observed. It is not clear at this point where this originates. Figure 13 shows the power spectral density (PSD) of the lift variation with the frequency for the URANS and DDES results. There is a pronounced peak in the PSD distributions at nondimensional frequencies of 0.06 and 0.08 for the URANS and DDES results, respectively, showing that DDES predicts a higher buffeting frequency compared to URANS. The corresponding Strouhal frequencies ($St = 2\pi f c/U_\infty$) for the URANS and DDES are about 0.37 and 0.49, respectively. The DDES predicted buffet frequency is closer to the experimental value of 0.47, while the peak amplitudes in the PSD distributions are about the same for both simulations.

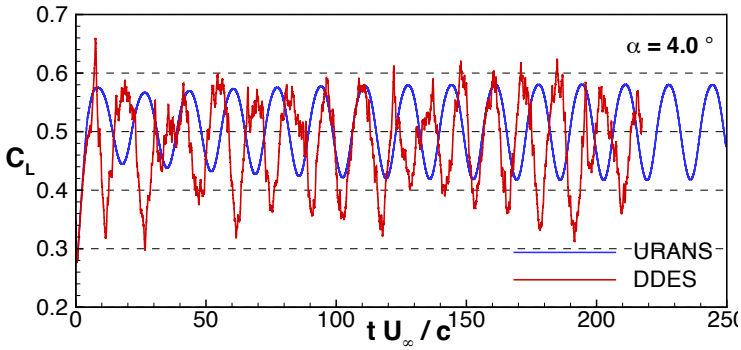

Fig. 12 Variation of lift coefficient with time for $\alpha = 4.0°$.

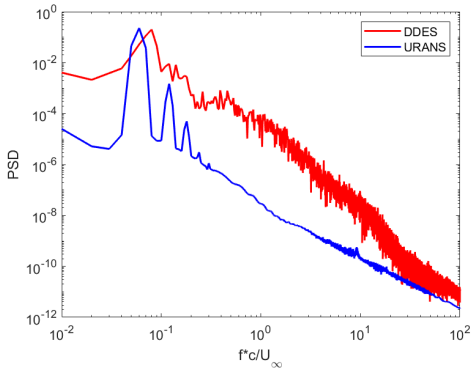

Fig. 13 Power spectral density (PSD) variation of the lift coefficient with frequency ($\alpha = 4.0°$).

Figures 14-16 show flow features observed during one cycle of lift oscillations. Figures 14(a-d) depict the spanwise vorticity contours in a crossplane at four time sequences t = 0T, 1/4T, 1/2T. and 3/4T. These time histories are shown in the Fig. 12. Figure 14(a) displays the vorticity distributions at the maxium point of the lift distributions, and Fig. 14(c) shows the results at the minimum point of the lift distributions. The flow field corresponding to Fig. 14(b) (t=1/4T) is displayed on the surface of the wing and on the spanwise boundary plane in Fig. 15. The instantaneous skin friction coefficient is plotted on the surface of the wing and *u*-velocity contours are plotted in the boundary plane. The grey area on the surface reflects the negative skin friction. It shows that the flow is separated from the shock to the trailing edge, corresponding to the large separated region in the boundary plane. This was seen during the entire cycle of buffeting and means that the flow remains separated during the entire cycle; however, the size of the separation changes during the cycle as seen in Figs. 14(a-c). Associated with the separation, a shear layer is formed above the recirculation zone. This region is expected to be in the LES mode. Figures 14(a-c) show the breakdown of the shear layer and formation of strong vortex structures.

Figures 16(a), (b), and (c) show the shielding function f_d in the DDES formulation, the boundary layer velocity profiles at different stations, and the eddy-viscosity, respectively, at the instant of time t =1/4T (Fig. 14b). The function $f_d = 0$ region is in the RANS mode and the function $f_d = 1$ region is in the LES mode. The RANS region is confined to a thin region near the wall on the order of 0.005 in height at every station except near the shock where the RANS region extends up to 0.01. In Fig. 16(b), a line is drawn at a height of 0.01 to show the boundary layer in the RANS mode. Most of the shear layer region is in the LES mode, which is expected from the design of the DDES method. These observations agree with the DDES of Grossi (2014), but some of the recirculation regions are also in the LES mode very near the wall. The eddy viscosity from DDES is on the order of 100-200 compared to URANS, which predicts a value of ~5000 at this angle of attack. This reflects the previous observation that most of the boundary layer downstream of the shock is in the LES mode and the modeled stresses are small compared to the resolved stresses.

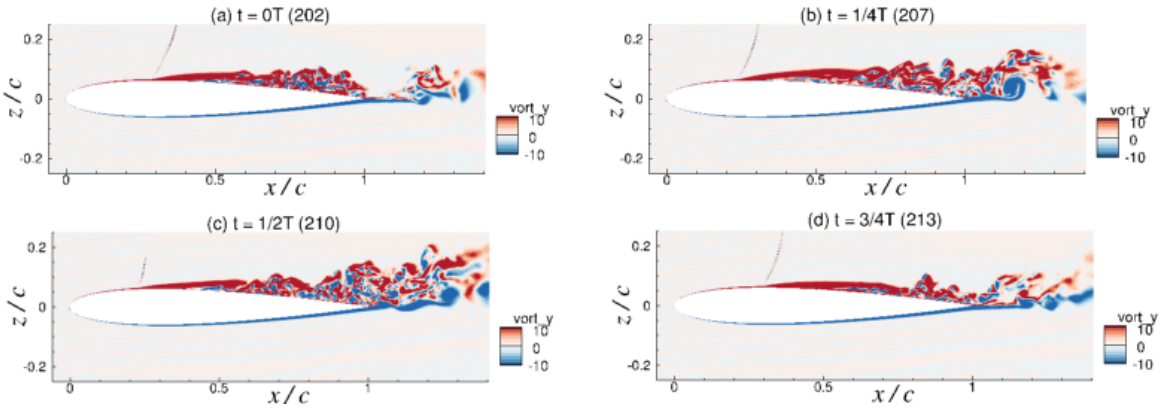

Fig. 14 Spanwise voricity contours during one cycle of the buffetting for $\alpha = 4.0°$.

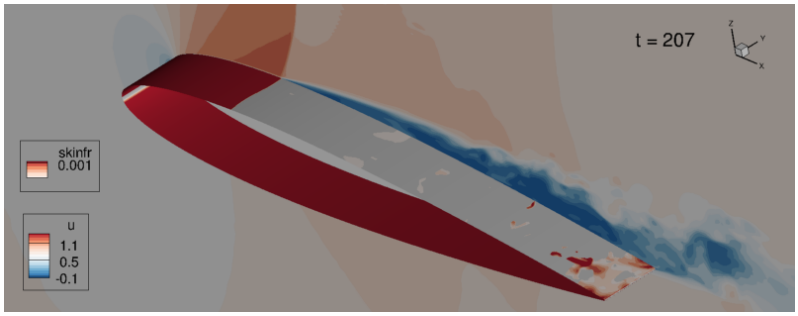

Fig. 15 Skin friction on the surface and u-velocity contours in the spanwise boundary plane ($\alpha = 4.0°$).

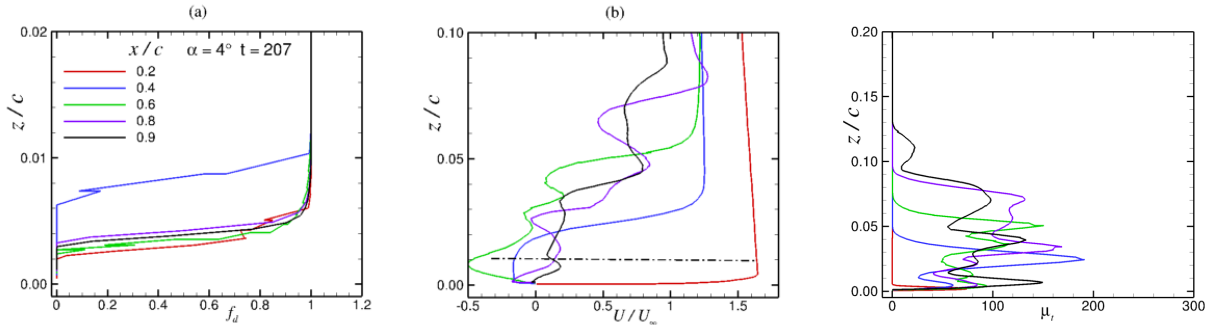

Fig. 16 Boundary layer functions at an instant t=1/T. (a) Shielding function f_d , (b) the bounday layer velocity profiles, and (c) the eddy-viscosity ($\alpha = 4.0°$).

Figures 17(a) and (b) show the time-averaged *u*-velocity contours and pressure distributions. Figure 17(a) shows that the flow is separated from the root of the shock to the trailing edge of the wing. Comparing these results to the mean velocity contours from the URANS solutions shown in Fig. 6(b), the separation bubble predicted by DDES is thicker and longer compared to the URANS result. Whether this is due to the lack of resolved turbulent stresses near the foot of the shock has to be explored further. In Fig. 17(b), the pressure distribution obtained using URANS at angle of attack of 4 degrees is plotted with the DDES results. Compared to the URANS solutions, the shock starting point occurs further upstream. The shock is more smeared due to the shock oscillations. A plateau is seen on the downstream part of the distribution starting at $x/c \sim 0.35$. This is due to the large separation bubble predicted by the DDES. Similar pressure distributions with a plateau downstream of the shock were also observed in the IDDES prediction of flow over the OAT15A airfoil.[32]

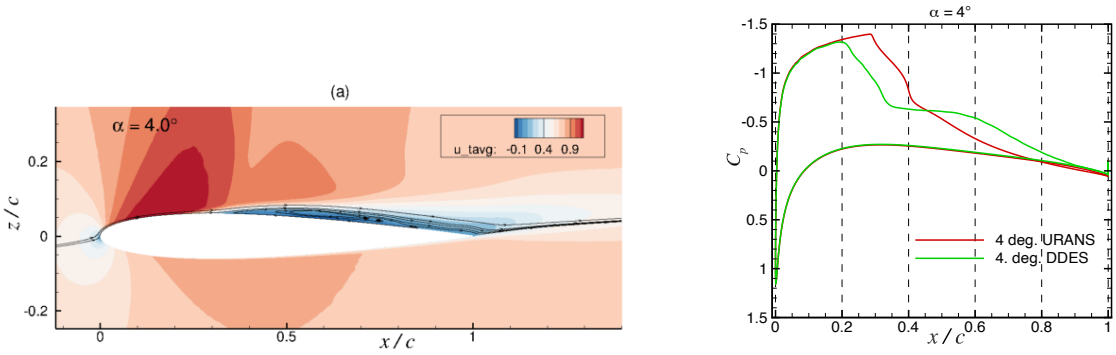

Fig. 17 Time-averaged (a) u-velocity contours and the streamlines and (b) pressure distributions.

Figures 18(a) and (b) display the contours of the root mean square (rms) of the pressure and *u*-velocity fluctuations, respectively, for an angle of attack of 4.0 degrees. The contours are like that observed in the URANS, Figs. 8(a, b). As expected, larger pressure fluctuations are observed across the shock oscillation region. Pressure fluctuations are also observed downstream of the shock above the wing. The structure of the rms for the pressure agrees well with the eigenfunctions distributions computed using the global stability analysis.[20] The width of the shock oscillations on the surface of the wing spans about 0.19 to 0.34, whereas it spans about 0.29 to 0.40 in the URANS. Due to the instability of the shear layer formed by the separation bubble, large velocity fluctuations are observed above the wing downstream of the shock. Figures 19(a) and (b) display the mean velocity and the turbulent normal stresses obtained from DDES, respectively. The mean flow profiles obtained from URANS are also included for comparison. The plots clearly show that the boundary layer profiles predicted by DDES are thicker than the URANS results. It is also seen that velocities inside the separation region are larger in DDES. The DDES results for the OAT15A airfoil[11] did not show significant differences in the boundary layer profiles between the URANS and DDES results. Figure 19(b) depicts the resolved and the model part of the normal stresses obtained from DDES. The modeled stresses are much smaller as expected compared to the resolved stresses in the most part of the boundary layer. The resolved stresses from the DDES are about two times higher than that from the URANS results.

As discussed in the introduction, one of the hypotheses proposed to explain the sustained oscillations of the shock is that the acoustic waves generated at the trailing edge by the eddies coming from upstream boundary layer propagate upstream towards the shock and perturb the shock. Figure 20 shows the instantaneous dilatational field emanating from the trailing edge. It is seen that the acoustic waves are indeed impinging on the shock. This has also been observed in other DDES and WMLES predictions.[10, 14, 32]

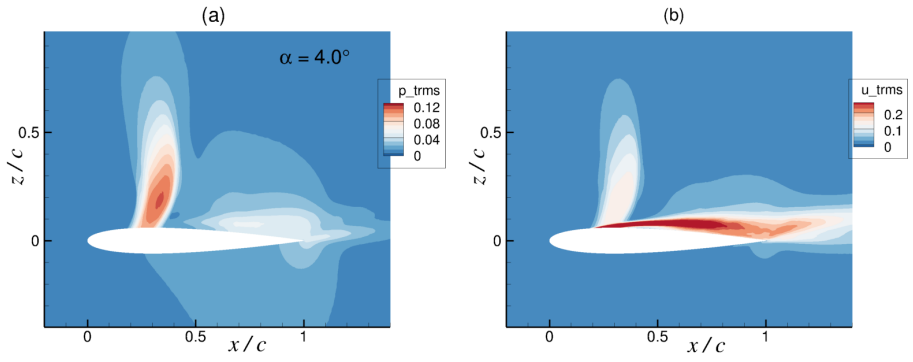

Fig. 18 Root mean square of (a) pressure and (b) u-velocity oscillations at $\alpha = 4.0°$.

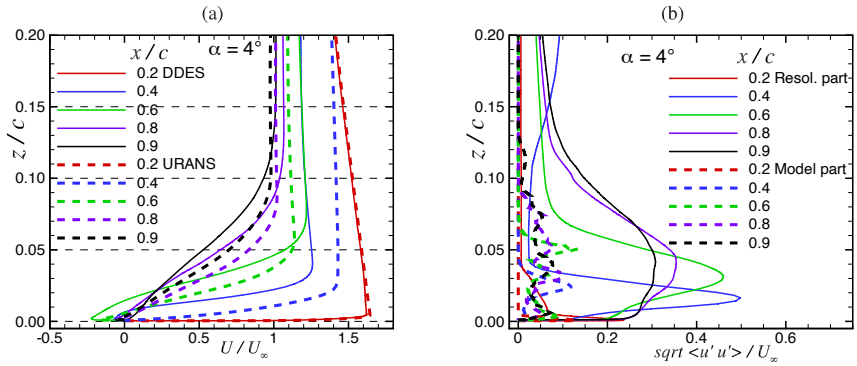

Fig. 19 Profiles of (a) mean u-velocity and (b) normal turbulent stresses at $\alpha = 4.0°$.

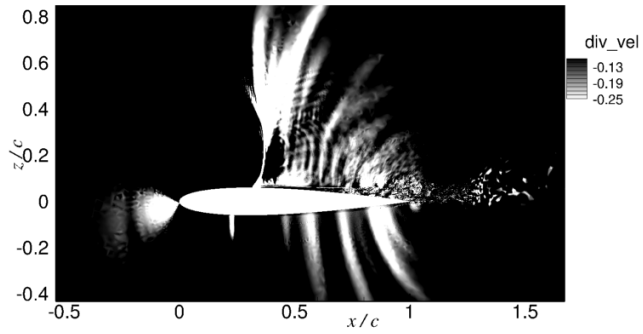

Fig. 20 Instantaneous dilatational field emanating from the trailing edge at $\alpha = 4.0°$.

It was noted above that the URANS simulations resulted in steady solutions until an angle of attack of 3.8 degrees using the SA model with the compressibility correction. URANS results for 3 degrees angle of attack were shown in Fig. 6(a). Figure 7(a) shows the pressure distributions for the 2 degrees angle of attack. DDES was performed at 2 and 3 degrees angle of attack using the same grid with the spanwise domain of 0.10c and 51 grid points in that direction and the same time step of $(U_\infty/c)dt$ = 0.00075.

Figure 21 displays the variation of the lift with time for an angle of attack of 2 degrees. A steady solution is obtained using DDES. It is seen that the computed lift coeffient is lower than that predicted by the URANS. The lift coefficients computed using DDES and URANS are approximately 0.30 and 0.37, respectively. The pressure distribution obtained from DDES (Fig. 7(a)) shows that the predicted shock location is upstream of the RANS value. This causes the lift coefficient to be lower than the RANS value. Similar observations were made in the analysis of IDDES results for the flow over the NACA0012 airfoil at 2 degrees angle of attack.[12]

Figure 22 displays the variation of the lift with time for 3 degrees angle of attack. The results from the URANS are also included in the figure. The behavior of the solution is much different than that obtained from the URANS. The lift curve is oscillatory with a fixed period and the average lift is almost 0.10 less than the URANS result. Figures 23(a) and (b) depict the spanwise vorticity contours when the shock is at the furthest downstream and upstream locations, respectively. The strong shear layer that forms at the root of the shock persists for a long distance before it breaks down into turbulence near the trailing edge. Figure 24(a) shows the shielding function distributions at different streamwise stations x/c = 0.2, 0.4, 0.6, 0.8, and 0.9. These lines are at a constant spanwise plane z/c = 0.05. Figure 24(b) displays the instantaneous velocity profiles. In Fig. 24(b) a line is drawn at a height of 0.01 to show the boundary layer in the RANS mode. It can be seen that the boundary layers at x/c = 0.2 and 0.4 are in the RANS mode and most of the boundary layers at x/c = 0.6, 0.8, and 0.9 are in the LES mode. At this instance, no separation is observed in this plane. Figure 25(a) shows the time-averaged u-velocity profiles and the streamlines. A thin separation bubble is observed from $x/c \sim 0.64$ to 0.85. Figure 25(c) displays the time-averaged pressure distributions. The pressure distribution predicted by DDES is quite different from the URANS results and shows the shock located further upstream.

Since the overall results from DDES differ from the URANS predictions, two additional DDES computations were made for this angle of attack with a narrower and a wider spanwise domain with the same number of grid points. The narrower domain was set to half the size of 0.05c and the wider domain was set 0.25c. The reason for selecting a narrower domain is to resolve the LES part with double the resolution. The wider domain is selected to increase the shielded RANS region near the wall to shield the separation region near the root of the shock within the RANS region. However, this will reduce the resolution of the LES region. The variations of the lift coefficients are shown in Fig. 22. The results from the narrower domain of 0.05c is about the same as that for the original domain of 0.10c. But with the wider domain of 0.25c, the lift variation follows the URANS results. The pressure distributions obtained from DDES are plotted in Fig. 25(c). The pressure distributions with the narrower domain are about the same as the original case. However, the pressure distribution with the wider domain came closer to the URANS solution. The shock is still located upstream. There is also a flat region in the presssure distribution implying a separation bubble downstream of the shock. The time-averaged *u*-velocity and the streamlines are shown in Fig. 23(b). As expected from the pressure distribution, a large separation bubble appears downstream of the shock. These simulations show the difficulties in predicting the flow field with separation bubbles using DDES methodology. The zonal methods (Deck et al. 2007)[10] may yield better prediction by protecting the shock boundary layer interaction region in the RANS model, but one will have to decide where to switch from RANS to LES.

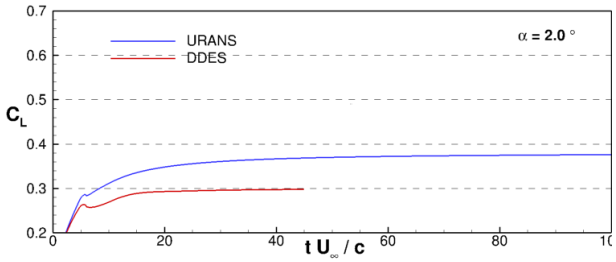

Fig. 21 Variation of lift coefficient with time at $\alpha = 2.0°$.

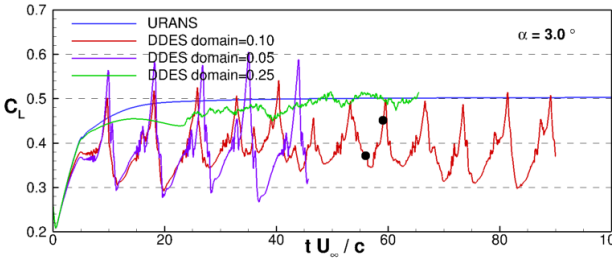

Fig. 22 Variation of lift coefficient with time at $\alpha = 3.0°$.

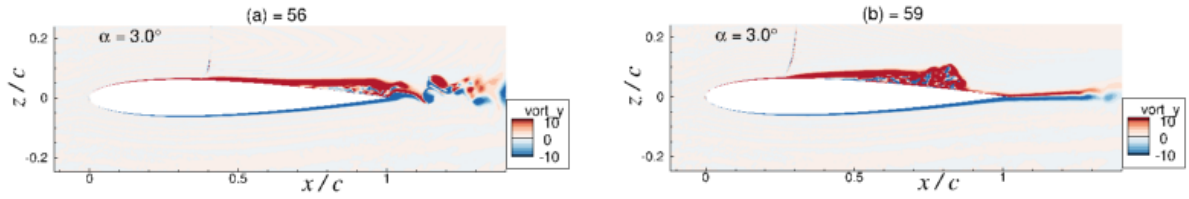

Fig. 23 Spanwise vorticity contours when the shock is furthest (a) downstream and (b) upstream for $\alpha = 3.0°$.

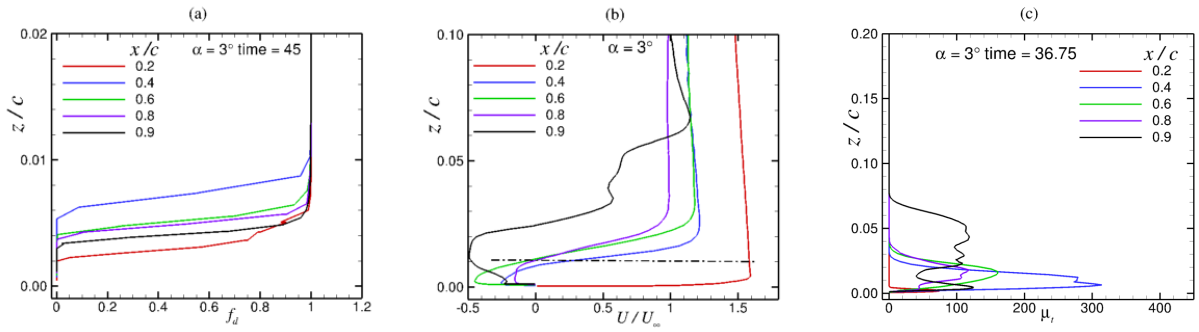

Fig. 24 Boundary layer functions at an instant t=45. (a) Shielding function f_d , (b) boundary layer velocity profiles, and (c) eddy-viscosity ($\alpha = 3.0°$); Note different vertical scales for (a), (b) and (c).

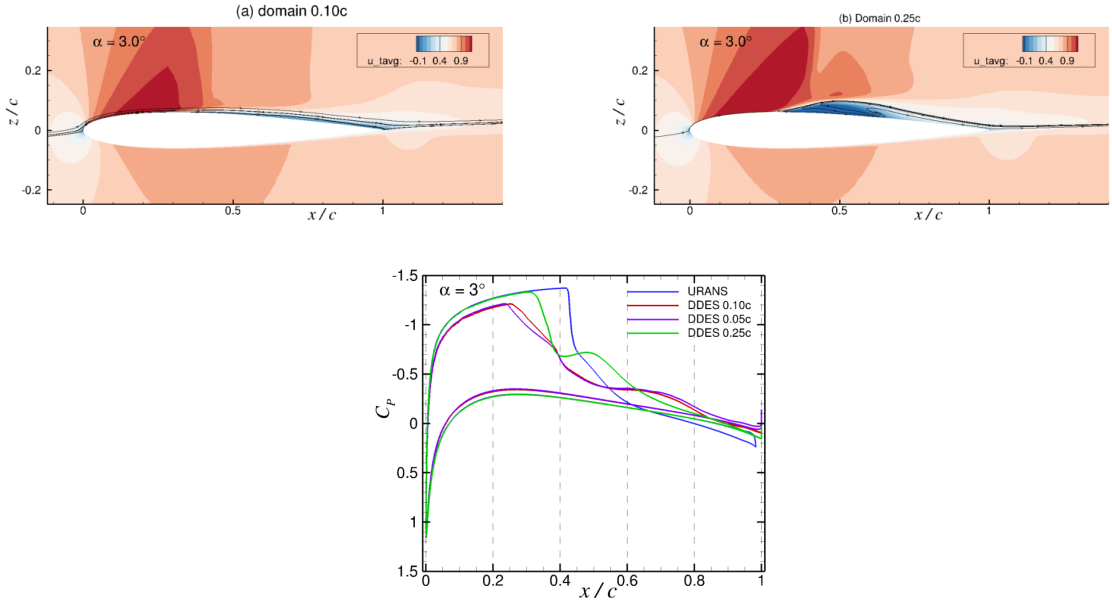

Fig. 25 Time-averaged u-velocity contours and streamlines for three DDES domain widths (a) 0.10c, (b) 0.25c, and (c) pressure distributions ($\alpha = 3.0°$).

C. WMLES

WMLES are performed for the same conditions using FUN3D to assess its ability and the requirements to predict buffet onset. WMLES capabilities have been recently added in FUN3D and assessed for canonical 2D geometries and for 3D geometries.[23] The WMLES implementation largely follows the methodology described in Kawai and Larsson (2012).[33] At each time step, the LES equations are first solved on a coarser grid. The first grid point off the wall is used as the exchange location at which the flow-field variables are extracted and are transferred to the wall model computations. The extracted solutions serve as input to a simple equilibrium wall model,[34] which is used to determine the local shear stress at each grid point on the solid-wall surface. Once the shear stress is determined, it is used to compute boundary-face fluxes required for evaluating the residuals at the boundary grid points. The UMUSCL reconstruction parameter, κ, is set to 0.9 in the domain to minimize the numerical dissipation, and to 0.5 for the cells attached to the walls for numerical stability. The Van Albada limiter is turned on in shock-dominated regions as identified by a Ducros sensor.[35] The solution is advanced in time using 2nd-order backward-Euler implicit scheme.

Figure 26 shows the unstructured grid topology used in the simulations. A C-type grid covers the wing and the wake with hexahedral cells. A fine mesh is patched on the upper surface to capture the expected shock movement. The height of the first grid point varies between 1 - $7\times10^{-4}c$, and the streamwise grid spacing over the wing varies from $3 - 7\times10^{-4}$. The 2D grid is extruded along the spanwise direction to a domain size of $0.02c$. Note that the spanwise extent is likely too narrow and needs to be wider. The focus here is on assessing the grid resolution requirements to

predict buffet using WMLES. The grid is uniform in the spanwise direction, consisting of 31 points with a spacing of 6.7×10^{-4} c. The grid contains 0.37M nodal points in a single plane, and 12M points in total. This is referred to as the baseline grid, while a finer grid with twice the resolution in the spanwise direction is also used. A nondimensional time step of $\Delta t\ (U_\infty/c) = 0.00068$ is used in the simulation, with 5 subiterations per timestep. This gave approximately two orders of reduction in the residual magnitude. The effects of increasing subiterations and reducing time step remains to be examined.

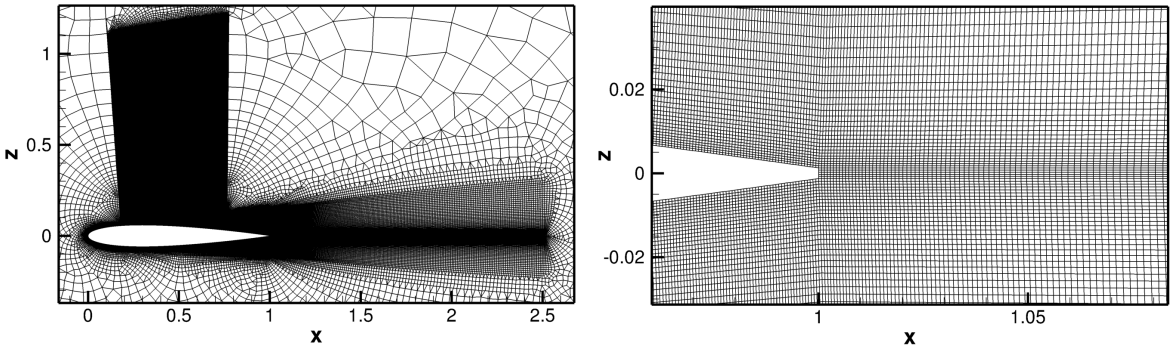

Fig. 26 Grid topology used for the WMLES predictions.

WMLES results are reported for angles of attack of 2, 4, and 4.5 degrees. Note that the 2 degree angle of attack calculation was performed at Re_c=11.7 million, and compared with experimental data at the same *Re*. URANS and DDES predicted buffet starting at about 4 degrees. Figure 27 depicts the variation of the lift coefficients predicted by the WMLES using the baseline grid for the three angles of attack. The lift curve for the 2 degree case displays a steady solution as expected. The lift coefficient from the WMLES is about 0.37 compared to 0.38 predicted by the URANS. The lift curve for 4 degrees did not display any buffeting contrary to the results obtained using URANS and DDES. The lift coefficient reaches a mean value of 0.67, which is much larger than the value of 0.50 predicted by the URANS. The lift curve for the 4.5 degrees shows buffeting, with a time period of about 20 c/U_∞ and an average lift coefficient of about 0.65, both of which are larger than the value predicted by URANS. While URANS indicated a sinusoidal variation of the lift coefficient with a single dominant frequency (corresponding to buffet), WMLES indicates a more complex shape with higher secondary frequencies, especially over the region where the lift drops from the maximum value. These higher frequencies appear to correspond to acoustic waves in the flow, although it needs to be verified whether these are physical. On this baseline grid, buffeting also occurred at an angle of attack of 6 degrees (not shown) similar to the 4.5 degree case, which is contrary to the predictions of URANS.

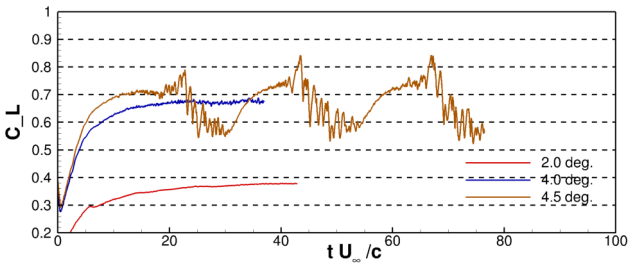

Fig. 27 Variation of lift coefficient with time for WMLES corresponding to $\alpha = 2.0°, 4.0°$ and $4.5°$ on the baseline grid.

To examine the effect of grid resolution on the results, a refined grid with twice the resolution was used in the spanwise direction, and identical resolution in the 2D plane. The boundary layer upstream of the shock did not contain sufficient resolved turbulence on the baseline grid for 4 degrees angle of attack. Note that the boundary layer thickness at x/c = 0.2 is about 0.004*c*, which corresponds to under 6 points within the boundary layer in the spanwise direction. This coarse resolution was unlikely to support resolved turbulence at this location, and hence the spanwise resolution was doubled. The variation of lift coefficient for 4 and 4.5 degrees angles of attack is shown in Figure 28 for the baseline and spanwise refined grids. Interestingly, the 4 degrees angle of attack result for the refined grid shows buffeting as expected, and has a lower lift coefficient compared to the baseline grid. The time period is about 18 c/U_∞, which is

close to the URANS value. For the 4.5 degrees angle of attack case, the buffeting onset starts earlier for the refined grid compared to the baseline grid, and the lift coefficient and time period are lower, but closer to the URANS values.

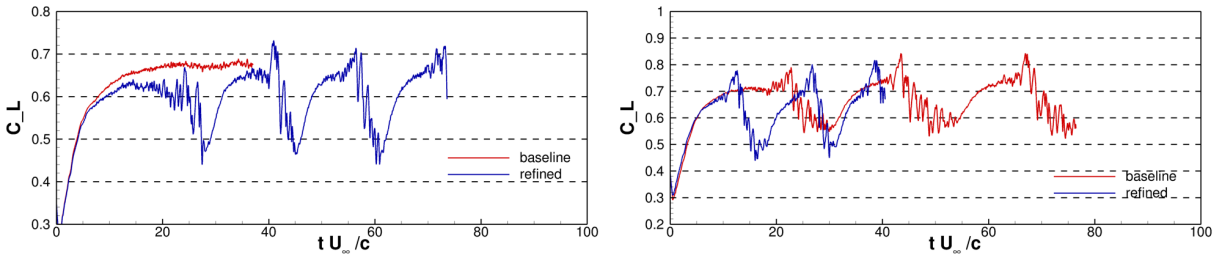

Fig. 28 Variation of lift coefficient with time for $\alpha = 4.0°$ (left) and $\alpha = 4.5°$ (right) degrees with the baseline and refined grid.

Figure 29 compares the time-averaged pressure coefficient from spanwise-refined WMLES grid result, with the experiment,[1] and URANS. The WMLES results agree well with the experiment at 2 degrees, except near the foot of the shock. The shock is less smeared compared to the experiment near the end of the shock region. At 4 and 4.5 degrees angle of attack, the WMLES result is close to the URANS result, with a slightly delayed shock location leading to an increased lift coefficeint.

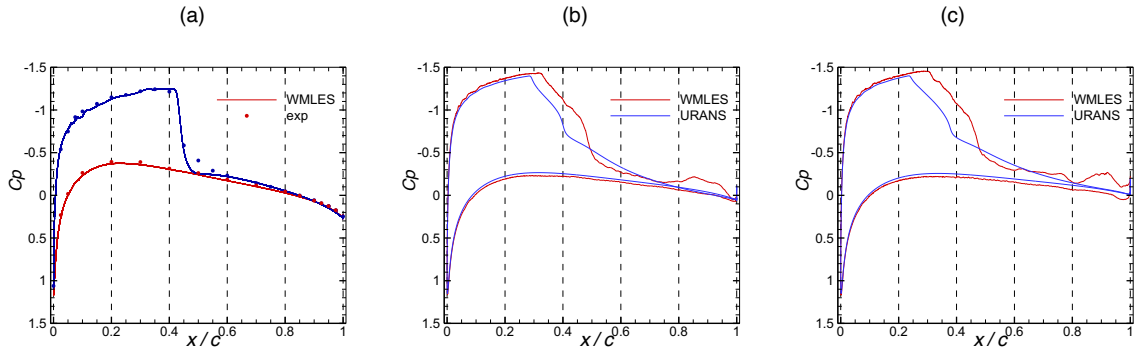

Fig. 29 Pressure coefficient distributions at different angles of attack, (a) $\alpha = 2.0°$, (b) $\alpha = 4.0°$, and (c) $\alpha = 4.5°$.

Figure 30 depicts the instantaneous horizontal velocity (u), dilatation and density gradient contours for 4 and 4.5 degree angle of attack on the spanwise refined grid. The time instants shown in the figure correspond to $(U_\infty/c)t =$ 46 and 27, for the 4 and 4.5 degrees angles of attack, respectively. These time instants also correspond to the minimum and maximum lift coefficient for 4 and 4.5 degrees angles of attack (see Figure 28). While the separation bubble is small for 4 degrees, a large bubble is seen between $x/c = 0.3$ and 1.0 on the top surface of the airfoil for the 4.5 degrees case at the instants shown. The dilatation contours are qualitatively similar to previous WMLES results[14] and show the presence of acoustic waves emanating from the boundary layer eddies, shock and separation regions. Finer scale vortices and acoustic waves are visible in the WMLES results as compared to DDES and URANS results discussed before. Stronger waves are seen for the 4.5 degrees case along with multiple shocks. Instantaneous density gradient contours depict the shock and shear layers in the flow, indicating the presence of multiple separation shear layers for the 4.5 degrees case.

Overall, the WMLES results are encouraging, especially on the spanwise refined grid which predicts buffet at 4 and 4.5 degrees angles of attack. The results are qualitatively consistent with URANS and DDES, with the dominant frequency matching closely. Investigation of the fine grid at lower and higher angles of attack, and further analyses of the results are necessary to understand the complex features present in this flow. Also, the effects of spanwise domain extent, grid refinement (in all directions), reduced time step, and increased subiterations on the buffet predictions are necessary and will be explored in the future.

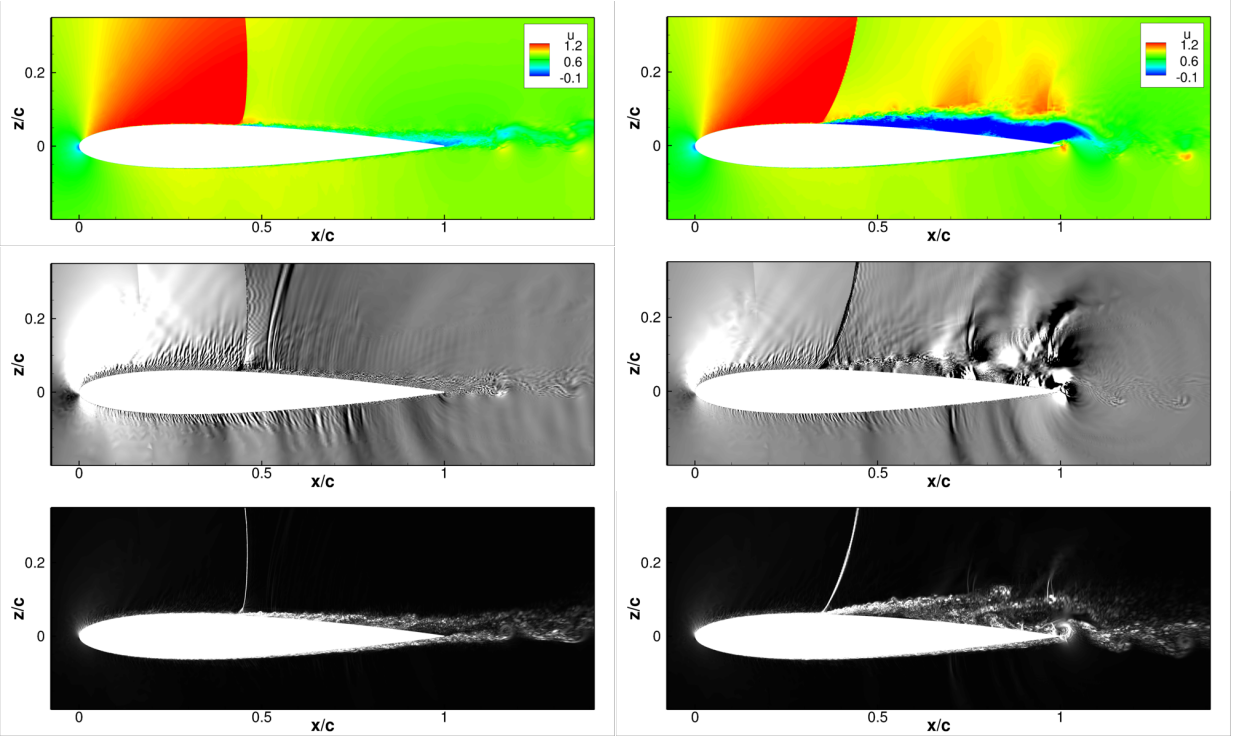

Fig. 30. Instantaneous *u*-velocity (top), dilation (center) and density gradient magnitude (bottom) contours for $\alpha = 4.0°$ (left) and $\alpha = 4.5°$ (right).

IV. Conclusions

Simulations were performed of the flow over an NACA0012 airfoil at a transonic Mach number of 0.75 and Reynolds number of 10×10^6 using URANS, DDES, and WMLES. The unstructured FUN3D code and the Spalart-Allmaras (SA) turbulence model with the compressibility correction were used for the simulations. The URANS results revealed a steady solution for an angle of attack of 3.8 degrees. The transonic buffet was observed for a narrow range of angles of attack between 4 and 5.5 degrees. The periods of shock oscillations were found to be very long, on the order of 15–16 times the convective time c/U_∞. The predicted shock oscillation frequency was slightly lower than that measured in the experiment.[1] The instantaneous velocity contours showed merging and splitting of two separation bubbles that appeared at the root of the shock and near the trailing edge. The time-averaged velocity field showed a separation bubble extending from the root of the shock to the trailing edge at an angle of attack of 4.5 degrees. These conclusions in general agree with other URANS simulations performed for the 2D airfoils.[2, 7-9] With appropriate turbulence models, the transonic buffet onset and the frequencies could be predicted reasonably well compared on the experiments. The contours of the pressure oscillation rms revealed large intensity across the shock oscillation region. Disturbances were also observed above the boundary layer. The distribution of the pressure rms is similar to the eigenfunction shape obtained from the global stability analysis. The boundary layer thickness increases by 5–10 times downstream of the shock compared to the incoming boundary layer. The eddy viscosity increases from about 100–200 upstream of the shock to about 1000–5000 downstream of the shock.

DDES was performed using the SA-based DDES model at 2, 3, and 4 degrees angles of attack. The simulation results at 4 degrees showed shock oscillations similar to that observed in the URANS. The oscillations are not as periodic as observed in DDES results for the OAT15A airfoil.[11] The instantaneous vorticity contours showed formation of a detached shear layer and the breakdown of this layer into small scales. The shielding function in the DDES formulation as expected showed that the boundary layer close to the wall is governed by the RANS and the outer layer above the wall is resolved by the LES. This also agreed with the observed very low eddy viscosity levels in the DDES compared to the URANS predictions. The power spectral density (PSD) analysis indicated a pronounced peak at a frequency closer to the measured frequency of oscillations. However, the time-averaged mean velocity and the pressure showed a larger separation bubble compared to that predicted by the URANS. This was also observed in other studies using DDES and IDDES .[10-12, 32]

DDES was also used to examine the flow at prebuffet onset angles of 2 and 3 degrees. The simulation at 2 degrees depicts a steady solution with the lift value lower than that predicted by RANS, and the predicted shock location is upstream of the experiment. The DDES performed at 3 degrees angle of attack with the same grid produced different results compared contrary to the URANS predictions. URANS yielded a steady solution with a thin, small bubble at the foot of the shock. DDES predicted the buffet, however the average lift was much lower than the URANS results at 3 degrees, and the time-averaged solution showed a very thin separation region.

Comparing the URANS and DDES, the results suggest URANS with an appropriate turbulence model predicts the buffet characteristics better than DDES. There are not many examples in the literature where DDES has been performed at pre-onset conditions to check the applicability of this method to such cases. The shear layer that forms at the foot of the shock persists for some distance before it breaks down to turbulence. Even the zonal methods that shield the shock boundary layer interaction region fail to predict the shock location and the pressure distributions correctly.[10]

WMLES was performed at three angles of attack: 2, 4, and 4.5 degrees, with a relatively narrow span of 0.02c. The pressure distributions and the lift coefficient agree well with the experiment at 2 degrees. WMLES did not predict the expected buffeting at 4 degrees angle of attack for the baseline grid, while it did at 4.5 degrees angle of attack. The lack of buffeting for the 4 degrees angle of attack case was traced to the lack of resolved turbulence in the thin boundary layer upstream of the shock. Doubling the spanwise resolution produced buffet for the 4 degrees case, which is consistent with experiment, and improved the lift and buffet time period for the 4.5 degrees case. While the present results are encouraging, the effects of domain spanwise width, grid resolution and time step on the flow characteristics need further examination.

Acknowledgments

This research is sponsored by the NASA Transformational Tools and Technologies (TTT) Project of the Transformative Aeronautics Concepts Program under the Aeronautics Research Mission Directorate (ARMD). The authors would like to acknowledge Behzad R. Ahrabi from the Boeing Research & Technology for providing the grids used in the URANS and DDES. The authors also thank Andrew Leidy for performing the PSD analysis using the MATLAB, Kyle Anderson for useful discussions, and Steve Woodruff , Pawl Chwalowski, and Philippe Spalart for feedback on the paper.

References

[1]MeDevitt, J. B., and Okuno, A. F., "Static and Dynamic Pressure Measurements on a NACA 0012 Airfoil in the Ames High Reynolds Number Facility," NASA TR NASA-TP-2485, 1985.
[2]Giannelis, N. F., Vio, G. A., and Levinski, O., "A Review of Recent Developments in the Understanding of Transonic Shock Buffet," *Progress in Aerospace Sciences*, Vol. 92, 2017, pp. 39–84. https://doi.org/10.1016/j.paerosci.2017.05.004.
[3]Lee, B. H. K., Self-Sustained Shock Oscillation on Airfoils at Transonic Speeds", Prog. Aerosp. Sci., 37 (2) (2001) 147-196.
[4]Benoit, B., and Legrain, I., "Buffeting Prediction for Transport Aircraft Applications Based on Unsteady Pressure Measurements," 5th Applied Aerodynamics Conference, AIAA Paper 1987-2356, 1987, pp. 225–235.
[5]Denegri, C. M., Jr., "Limit Cycle Oscillation Flight Test Results of a Fighter with External Stores," Journal of Aircraft, Vol. 37, No. 5, Sept. 2000, pp. 761–769. doi:10.2514/2.2696
[6]Jacquin, L., Molton, P., Deck, S., Maury, B., and Soulevant, D. "Experimental Study of Shock Oscillation Over a Transonic Supercritical Profile," AIAA Journal, Vol. 47, No. 9, 2009, pp. 1985–1994. doi:10.2514/1.30190
[7]Brunet, V., Computational Study of Buffet Phenomenon with Unsteady RANS Equations, 2003. https://doi.org/10.2514/6.2003-3679.
[8]Goncalves, E., and Houdeville, R., "Turbulence Model and Numerical Scheme Assessment for Buffet Computations," International Journal for Numerical Methods in Fluids, Vol. 46, No. 11, 2004, pp. 1127–1152. https://doi.org/10.1002/fld.777.
[9]Iovnovich, M., and Raveh, D. E., "Reynolds-Averaged Navier-Stokes Study of the Shock-Buffet Instability Mechanism," AIAA Journal, Vol. 50, No. 4, 2012, pp. 880–890. https://doi.org/10.2514/1.J051329.
[10]Deck, S., "Numerical Simulation of Transonic Buffet over a Supercritical Airfoil," AIAA Journal, Vol. 43, No. 7, 2005, pp. 1556–1566. https://doi.org/10.2514/1.9885.
[11]Grossi, F., Braza, M., and Hoarau, Y., "Prediction of Transonic Buffet by Delayed Detached-Eddy Simulation," AIAA Journal, Vol. 52, No. 10, 2014, pp. 2300–2312. https://doi.org/10.2514/1.J052873.
[12]Weiner, A., and Semaan, R., "Simulation and Modal Analysis of Transonic Shock Buffets on a NACA-0012 Airfoil", AIAA SciTech Forum, January 3-7, 2022, San Diego, CA.
[13]Nguyen, N. C., Terrana, S., and Peraire, J., "Large-Eddy Simulation of Transonic Buffet Using Matrix-Free Discontinuous Galerkin Method", AIAA J., 2002. https://doi.org/10.2514/1.J060459.
[14]Fukushima, Y., and Kawai, S., "Wall-Modeled Large-Eddy Simulation of Transonic Airfoil Buffet at High Reynolds Number," AIAA Journal, Vol. 56, No. 6, 2018, pp. 2372–2388. https://*doi.org/10.2514/1.J056537*.
[15]Lee, B. H. K., "Transonic Buffet on a Supercritical Airfoil," Aeronautical Journal, May 1990, pp. 143–152.

[16]Crouch, J. D., Garbaruk, A., Magidov, D., and Travin, A., "Origin of transonic buffett on aerofoils", Journal of Fluid Mechanics, Vol. 628, 2009, pp. 357-369.
[17]Edwards, R., and Chandra, S., "Comparison of Eddy Viscosity-Transport Turbulence Models for Three-Dimensional, Shock Separated Flow Fields," 25th AIAA Fluid Dynamics Conference, AIAA Paper 1994-2275, 1994.
[18]Anderson, K. W., and Bonhaus, D. L., "An Implicit Upwind Algorithm for Computing Turbulent Flows on Unstructured Grids", Computers Fluids, Vol. 23, No. 1, pp. 1-21, 1994.
[19]Anderson, W., Rausch, R., and Bonhaus, D. L., "Implicit/Multigrid Algorithms for Incompressible Turbulent Flows on Unstructured Grids," Journal of Computational Physics, Vol. 128, 1996, pp. 391–408, doi https://doi.org/10.1006/jcph.1996.0219.
[20]Roe, P. L., "Approximate Riemann Solvers, Parameter Vectors, and Difference Schemes," Journal of Computational Physics, Vol. 43, 1981, pp. 357–372, doi: https://doi.org/10.1016/0021-9991(81)90128-5.
[21]Burg, C. O. E., "Higher Order Variable Extrapolation for Unstructured Finite Volume RANS Flow Solvers," AIAA Paper 2005-4999, 2005.
[22]Van Leer, B., "Towards the Ultimate Conservative Difference Scheme, V. A Second Order Sequel to Godunov's Method", J. Comput. Physics, Vol. 32, 1979, pp. 101-136.
[23] Wang, Li, Anderson W. Kyle, Nielsen Eric J., Balakumar, P., Park, M. A., Carlson, J. R., Iyer, P., and Diskin, B., "Wall-Modeled Large-Eddy Simulations for High-Lift Configurations using FUN3D", AIAA Sci Tech Forum, January 3-7, 2022, San Diego, CA.
[24]Spalart, P. R., and Allmaras, S. R., "A one-equation turbulence model for aerodynamic flows", La Recherche Aerospatiale, Vol. 1, Jan. 1994, pp. 5-21.
[25]Shur, M. L., Strelets, M. K., Travin, K. A., and Spalart, P. R., "Turbulence Modeling in Rotating and Curved Channels: Assessing the Spalart–Shur Correction", AIAA Journal, Vol. 38, No. 5, May 2000.
[26]Mani, M., Babcock, D. A., Winkler, C. M., and Spalart, P. R., "Predictions of a Supersonic Turbulent Flow in a Square Duct", AIAA Paper 2013-0860, 2013.
[27]Spalart, P. R., "Trends in Turbulence Treatments", AIAA Paper 2000-2306, 2000.
[28]Raghunathan, S., Mitchell, R. D., and Gillan, M. A., "Transonic Shock Oscillations on NACA0012 Aerofoil," Shock Waves, Vol. 8, 1998, pp. 191–202.
[29]Spalart, P. R., Jou, W.-H., Strelets, M., Allmaras, S. R., "Comments on the Feasibility of LES for Wings and on RANS/LES Approach", in Proceedings of the first AFOSR international conference on DNE/LES, edited by C. Liu and Z. Liu. Greyden Press, Columbus, OH, 1998, pp. 137-147.
[30]Vatsa, V. N., Lockard, D. P., and Spalart, P. R., "Grid Sensitivity of SA-Based Delayed-Detached-Eddy-Simulation Model for Blunt-Body Flows", AIAA Journal, Vol. 55, No. 8, August 2017.
[31]Spalart, P. R., Deck, S., Shur, M. L., Squires, K. D., Strelets, M. K., and Travin, A., "A New Version of Detached-Eddy Simulation, Resistant to Ambiguous Grid Densities", Theoretical and Computational Fluid Dynamics, Vo. 20, 2006, pp. 181-195.
[32]Huang, J., Xiao, Z., Liu, J., and Fu, S., "Simulation of Shock Wave Buffet and Its Suppression on an OAT15A Supercritical Airfoil by IDDES," Science China Physics, Mechanics, and Astronomy, Vol. 55, No. 2, 2012, pp. 260-271.
[33]Kawai, S., and Larsson, J., "Wall-Modeling in Large Eddy Simulation: Length Scales, Grid Resolution, and Accuracy", Physics of Fluids, Vol. 24, No. 1, Jan. 2012, pp. 015105-1 to 015105-10.
[34]Spalding, D. B., "A Single Formula for the "Law of the Wall"," J. Appl. Mech., Vol. 28, No. 3, 1961, pp. 455–458.
[35]Ducros, F., Ferrand, V., Nicoud, F., Weber, C., Darracq, D., Gacherieu, C., & Poinsot, T., "Large-eddy Simulation of the Shock/Turbulence Interaction." *Journal of Computational Physics*, *152*(2), 517-549.